Time-Resolved, Confocal Single-Molecule Tracking of Individual Organic Dyes and Fluorescent Proteins in Three Dimensions

Jason J. Han,[†] Csaba Kiss,[‡] Andrew R. M. Bradbury,[‡] and James H. Werner[†,*]

[†]Center for Integrated Nanotechnologies and [‡]Biosciences Division, Los Alamos National Laboratory, Los Alamos, New Mexico 87545, United States

ABSTRACT

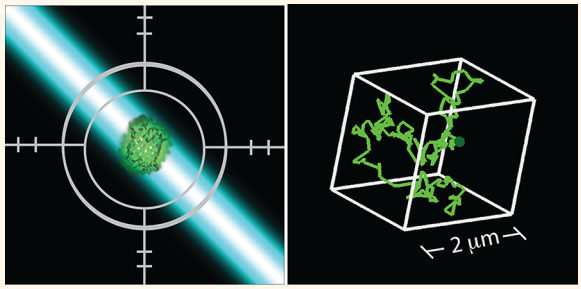

We demonstrate following individual fluorescent protein constructs and individual organic dyes as they diffuse in 3-D in solution at rates up to 1 $\mu m^2/s$ over distances of several micrometers in *X*, *Y*, and *Z*. Our 3-D tracking method is essentially a stage scanning confocal microscope that uses a unique spatial filter geometry and active feedback 200 times/s to follow fast 3-D motion. Here we detail simulations used to find optimal feedback parameters for following individual fluorescent proteins in 3-D and show that a wide range of parameters are capable of following individual proteins diffusing at 1 $\mu m^2/s$ rates. In addition, we experimentally show that through 3-D single-molecule tracking of a protein oligomer series (monomer, dimer, and tetramer) of the fluorescent protein Azami Green one can determine the protein oligomerization state. We also perform time-resolved spectroscopy (photon pair correlation measurements) during the measured 3-D trajectories. The photon pair correlation measurements show clear fluorescence photon antibunching, demonstrating that the trajectories are of single fluorescent molecules. We note that the rates of single-molecule diffusive motion we follow (approximately 1 $\mu m^2/s$) are comparable to or faster than many intracellular transport processes.

KEYWORDS: single molecule · tracking · confocal · three-dimensional · proteins

Single-particle tracking (SPT) is an important tool for directly visualizing the spatial trajectories of individual particles in various media, with applications ranging from exploring bacterial chemotaxis[1,2] to the study of material rheological properties[3] to the visualization of membrane dynamics[4−7] and motor protein kinetics.[8,9] The particles employed in these tracking experiments can be fluorescently labeled polystyrene beads that are micrometers in diameter,[8] large biomolecular complexes or whole bacteria labeled with multiple fluorophores,[1,2,4] or colloidal gold particles that are several hundreds of nanometers in diameter.[7,10] An important and growing subset of SPT experiments is single-molecule tracking (SMT).[11,12] Unlike SPT experiments,[13] SMT experiments are typically focused on the tracking of a single quantum emitter such as a single organic dye,[6] a single fluorescent protein,[14] or a single quantum dot[15,16] in time and space. For applications in biology, a biomolecule of interest (*e.g.*, protein, phospholipid, or DNA molecule) is typically labeled with a single optical probe to visualize its motion, with the measured spatial trajectory examined by an analysis of the molecule's mean squared displacement over time[5] or other more sophisticated analysis methods.[17] The simplest and most common SMT experimental method employs a wide-field imaging microscope and an array-based camera (*e.g.*, CCD) to image labeled molecules diffusing within a single, two-dimensional (2-D) detection plane.[18] This configuration is particularly well suited for imaging labeled membrane proteins and phospholipids that are constrained to diffusion across planar, supported model membranes[19−21] and flat regions of the complex plasma membrane landscape in live cells.[22,23] However, not all membranes are flat.[24,25] More importantly, many cellular functions such as intracellular signaling[26,27] and protein trafficking[28−30] occur over three dimensions across extended distances throughout the intracellular milieu. Visualizing these activities at the single-molecule level requires the ability to track

* Address correspondence to jwerner@lanl.gov.

Received for review June 29, 2012 and accepted September 7, 2012.

Published online September 08, 2012
10.1021/nn302912j

individual molecules over several micrometers in all three dimensions at biologically relevant diffusion (~1 $\mu m^2/s$) and transport (<1 $\mu m/s$) rates.

Current methods for three-dimensional (3-D) SMT[31] can utilize either passive, wide-field imaging-based techniques[32−40] or more sophisticated active, confocal feedback-based methods,[16,24,41−47] with also some effort at combining wide-field imaging in *XY* with active feedback in *Z*.[48] Passive, wide-field imaging methods employ wide-field illumination and fluorescence detection and, therefore, allow multiple single emitters to be imaged simultaneously as they diffuse into and out of one or more stationary (passive) detection planes. Typically, a temporal image stack is collected, and the 3-D trajectories of each fluorescent spot are constructed post-acquisition by employing localization algorithms to locate the centroid of each single emitter for each time step (image frame). Various methods such as point spread function (PSF) engineering[49,50] and astigmatic imaging[32,36,51] have been developed to encode the *Z*-position of out-of-focus emitters up to a depth of approximately ±1 μm axially above or below a given detection plane. When combined with multifocal plane detection,[33,35,37−39,48] wide-field imaging approaches can reconstruct 3-D trajectories spanning several micrometers in all three dimensions. In contrast to passive camera-based approaches, active, feedback-based tracking methods utilize confocal illumination and one or more single element detectors to physically track a single emitter in 3-D sample space. In this configuration, the fluorescence intensity from a single emitter that enters and diffuses within the confocal probe volume will fluctuate and scale according to its 3-D position within the approximate Gaussian excitation volume. The fluctuating fluorescence signal is used as real-time positional feedback to drive fast piezo scanners. The emitter is actively kept within the confocal probe volume by either scanning the probe volume through a stationary sample with piezo-driven galvanometer mirrors,[41,43,45,47] scanning the sample through a stationary confocal probe volume with a scanning piezo stage,[16,24,42,44,46] or a combination of both.[48] In either case, the use of fast piezo scanners enables active, physical tracking of a single molecule over several micrometers in all three dimensions. The emitter's 3-D trajectory is constructed in real-time without the need for post-acquisition processing and with millisecond to submillisecond temporal resolution typically not attainable by wide-field methods. In general, passive wide-field camera-based imaging methods focus on localization accuracy and have the advantage of imaging multiple single emitters simultaneously, whereas active confocal feedback-based methods place emphasis on temporal resolution and tracking over extended distances in all three dimensions. Several key advantages of the confocal approach over wide-field imaging-based techniques include (1) orders of magnitude less photodamage to live cells (as only a small spot is illuminated during the trajectory), (2) superior signal-to-noise ratio (SNR) in high background environments (due to the spatial filtering enabled by confocal detection), and (3) the ability to perform time-resolved spectroscopy (*e.g.*, photon pair correlations, fluorescence lifetime measurements, or fluorescence correlation spectroscopy) on the molecules being tracked.[16,41,45,46]

With one notable exception,[16] all demonstrations of 3-D SPT by confocal feedback have been performed on QDs or fluorescent polymeric nanoparticles, both of which are excellent probes for 3-D SPT because they provide an ample photon budget and thus a high per particle count rate, which yields a high SNR and enables collection of long (seconds to minutes) trajectories. Quantum dots, in particular, are excellent probes for labeling and tracking single biomolecules due in part to their superior photostability, which enables long track durations limited primarily by photoblinking,[46] though recent advances toward blinking-suppressed quantum dots are making progress in overcoming this limitation.[52,53] In addition, the use of commercially available QD bioconjugates allows for targeted labeling of specific intra- and extracellular proteins and organelles in live cells.[54−56] For example, we have followed the diffusion and endocytosis of membrane receptor-bound QD-labeled antibodies in live cells for tens of seconds using an active, real-time feedback-based confocal 3-D tracking microscope.[16]

Despite the advantages of QDs, the size of QD bioconjugates (typically 10−20 nm in diameter) precludes their use as labels for small (<100 kDa), soluble cytosolic proteins whose structure and/or function may be altered or obliterated by conjugation to such a large label. In these cases, labeling strategies may include expressing the protein of interest as a fusion to a fluorescent protein such as Green Fluorescent Protein (GFP),[57] creating a fusion with a short peptide marker encoded to bind to an exogenous and membrane-permeable organic dye-labeled synthetic probe (*e.g.*, SNAP-tag, FlAsH, ReAsH)[58,59] or creating a fusion of the protein of interest to a short GFP-derived peptide that requires complementation with the rest of GFP to be fluorescent.[60] The use of photoactivable fluorescent protein (FP) labels is a particularly attractive strategy since the concentration of photoactivated FPs at any given time can be optimized for single-molecule studies by controlling the intensity and duration of a photoactivating laser.[61,62] On the other hand, organic dyes are generally more photostable and yield higher per molecule photon count rates than FPs. In addition, oxygen-scavenging reagents designed to suppress photoblinking and photobleaching work particularly well with organic dyes.

While CCD imaging-based methods for 2-D tracking of individual fluorescently labeled biomolecules in live

cells are well-established, the ability to track soluble cytosolic proteins labeled with a single FP or organic dye over several micrometers in all three dimensions in live cells will represent a tremendous technical achievement toward elucidating the spatial interactions of these proteins with their complex surroundings. Toward this end, we have utilized our 3-D tracking methods[16,44,46] to demonstrate the tracking of single organic dye molecules, as well as monomeric Azami Green (mAG) fluorescent protein and its dimeric (dAG) and tetrameric (tAG) oligomers undergoing Brownian diffusion in glycerol–water mixtures at rates ranging from $D \approx 0.85$ to 0.35 $\mu m^2/s$. We note that while these rates (~1 $\mu m^2/s$) are less than the diffusion coefficient of a GFP-sized protein freely diffusing in the cytoplasm (~25 $\mu m^2/s$),[63] they are still faster (or comparable to) many intracellular transport processes, including diffusion of mRNA in the nucleus[64] or cytoplasm,[65] transport of proteins through the nuclear pore complex,[34,40] active motion driven by dynenin or kinesin,[9] motion induced by actin polymerization and depolymerization,[66] or diffusion of large (>1000 kDa) proteins in the cytoplasm where Brownian motion is hindered by macromolecular crowding.[67]

RESULTS AND DISCUSSION

Optimization of Tracking Parameters. Figure 1 depicts our 3-D confocal, feedback-based single-particle tracking microscope design, which has been described in detail elsewhere.[44] As illustrated, four single-photon avalanche diodes (SPADs) collect light *via* four optical fibers spatially arranged in orthogonal fiber optic pairs, with one pair axially separated from the other so as to form a tetrahedral detection volume in sample space. After each 5 ms track iteration, the photon counts on each SPAD are read out and sent to a feedback loop, which calculates the direction and magnitude over which to move the piezo stage in order to reposition the tracked molecule closer to the center of the confocal excitation probe volume. Optimal tracking parameters can depend upon the emission rate of the fluorophore, its diffusion coefficient, and the current alignment (*e.g.*, spacing between optical planes) of the tracking system. As such, we have found that optimizing the feedback parameters when switching between fluorescent reporters of varying emission rates (*e.g.*, FPs and organic dyes *versus* QDs) is important.

Originally, we performed simulations of our 3-D tracking microscope to find appropriate experimental parameters, such as the optimum separation distance between the two *Z* planes and the best effective magnification for the system.[42] In these original simulations, we employed an analytic approximation of the theoretically predicted model of the microscope's collection efficiency function (CEF) put forth by Enderlein,[68] with the CEF being a map of the relative photon counts collected from a dipole emitter for a given *X*, *Y*, *Z* location

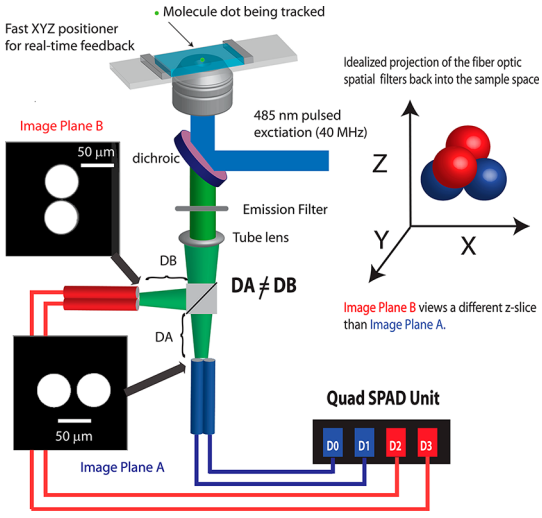

Figure 1. Schematic of the confocal 3-D tracking microscope optical configuration. The fiber optic pairs are configured to form a 3-D tetrahedron-like detection volume in sample space.

in the probe volume.[69] In a subsequent study, we repeated the simulations using an experimentally measured CEF in order to obtain optimal gain parameters for tracking red-emitting QDs.[46] Here, we have again used simulations to determine the optimal feedback parameters for tracking individual green-emitting fluorescent proteins and organic dyes undergoing Brownian motion with a diffusion coefficient comparable to 0.5 $\mu m^2/s$. Due to a change in detection color from red to green, we employed an experimentally measured 3-D CEF at a green emission wavelength.

The experimental CEF consists of a *Z*-image stack of raster-scanned *XY* images of an immobilized green-emitting QD. By linear interpolation of these *XYZ* raster scans, we are able to map out a measured photon probability distribution for every *XYZ* coordinate in sample space and can therefore predict the count rate of each detector for a fluorophore located at a given *XYZ* position in the probe volume. This knowledge, coupled to a measure of how the stage moves in response to a command (Supporting Information Figure S1), allowed us to test out different feedback parameters *in silico* prior to performing an actual tracking experiment in the laboratory.

For ease of comparison between all simulation runs, we set the initial *XYZ* coordinates at time $t = 0$ of both the stage and the molecule being tracked at the origin of the microscope system (*i.e.*, $(X_{M0},Y_{M0},Z_{M0}) = (X_{S0},Y_{S0},Z_{S0}) = (0,0,0)$, where subscripts "M" and "S" denote the molecule and stage positions, respectively). The molecule is then allowed to diffuse a distance $\sqrt{(2 \cdot D \cdot dt)}$ in each Cartesian coordinate direction, with equal probability of either "+" or "−" step direction for each axis. Here, *D* denotes the diffusion coefficient of the molecule and *dt* is a simulation time step of 100 μs. For each 100 μs time step, the count rate distribution across all

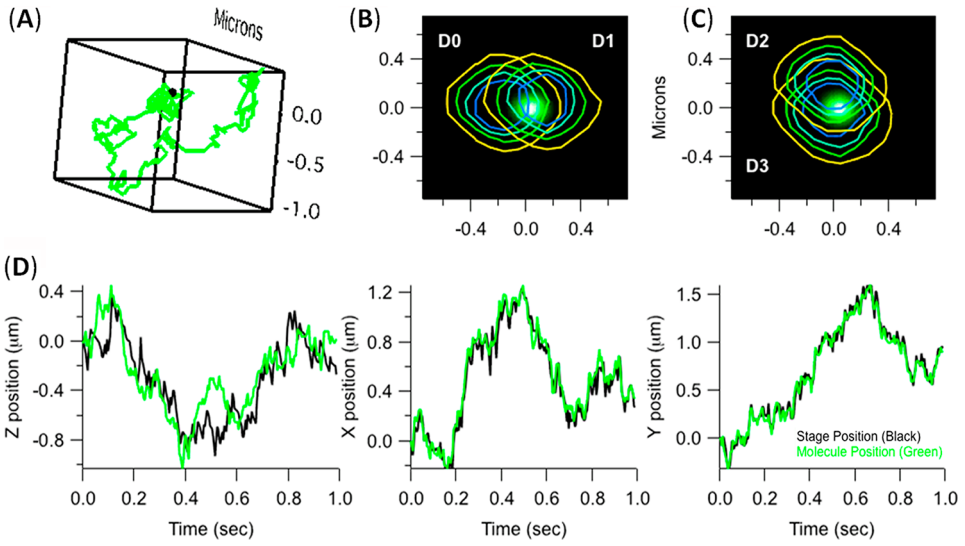

Figure 2. Example of a 1 s simulation of our tracking microscope following a fluorescent protein molecule diffusing at a rate of 0.5 $\mu m^2/s$. (A) Simulated 3-D trajectory of the molecule. (B,C) Molecule position (green spot) relative to the contours of the collection efficiency function (CEF) near $Z = 0$ for detector pairs D_0 and D_1 (B) and D_2 and D_3 (C). (D) Position of the molecule (green trace) *versus* the position of the stage (black trace) as a function of time for each Cartesian coordinate axis.

four detectors is weighted by the molecule's position in the experimentally measured 3-D CEF, with actual counts on each detector pulled from a Poisson distribution of the molecule's expected number of photons (N) for the 100 μs simulation time step. The counts on each detector are integrated over fifty 100 μs time steps (with the molecule also diffusing during each time step) for a total of 5 ms, after which the summed counts on all four detectors (D_0, D_1, D_2, D_3) are used as active feedback signals to determine which direction the stage must be moved in order to reposition the molecule closer to the center of the 3-D CEF in the simulation.

As described previously,[46] the direction and magnitude of a given 3-D stage translation is based upon proportional integral differential (PID) principles, with step size (SS) and direction (+ or −) for each axis given by

$$SS_X = K_X \cdot (D_0 - D_1)/(D_0 + D_1)$$

$$SS_Y = K_Y \cdot (D_2 - D_3)/(D_2 + D_3)$$

$$SS_Z = K_Z \cdot [(D_0 + D_1) - (D_2 + D_3)]/(D_0 + D_1 + D_2 + D_3)$$

where K_X, K_Y, and K_Z are gain parameters. On the basis of the four detector counts obtained in the first 5 ms interval, we issue a command at the start of the next 5 ms simulation cycle to move the stage using the above step sizes, SS_X, SS_Y, and SS_Z. The stage and molecule positions are then updated every 100 μs using a realistic model of the step response of the *XYZ* piezo stage (Supporting Information Figure S1) for the stage motion and a random walk for the molecule position as discussed above. The difference in coordinate values of the stage and molecule (*i.e.*, $[X_M - X_S]$, $[Y_M - Y_S]$, $[Z_M - Z_S]$), combined with the measured CEF of the system, is again used to obtain the counts on each detector for each 100 μs time interval. This process is repeated for 50 intervals of 100 μs, with the integrated counts on each detector again summed for a 5 ms period. At the end of this 5 ms period, the integrated counts on each detector are again used to decide which direction, as well as how far, to move the stage. Simulations are run for a finite time period (typically 1−10 s) or until the molecule is lost (the counts fall below a threshold value in the simulation).

Figure 2A shows a single 1 s simulated 3-D trajectory of a molecule with a diffusion coefficient of 0.5 $\mu m^2/s$. In Figure 2B,C, the *XY* position of the molecule (green spot) at an arbitrarily chosen time point in its trajectory is plotted against the photon probability distribution contours of the experimentally measured CEF near the $Z = 0$ image plane for detector pairs (D_0, D_1) and (D_2, D_3). The molecule's positional offset relative to the centers of the D_0-D_1 and D_2-D_3 detector pairs provides a visual representation of the direction and magnitude of the *X* and *Y* step sizes required to reposition it back into the center of the probe volume. Figure 2D shows the *XYZ* components of the 3-D trajectory in Figure 2A overlaid with the stage response as it tracks the molecule with K_X, K_Y, and K_Z gain values of 0.35, 0.35, and 0.75, respectively. As can be seen, the stage position more or less faithfully tracks the molecular position for this one simulation run. Inspection of this one graph shows that our *XY* tracking accuracy is superior to our *Z* tracking accuracy, a finding we have previously confirmed experimentally.[16] This and two other simulation runs at the same *K* values are shown as movies in the Supporting Information (supporting movies S1−S3).

While a single simulation run with a given set of *K* values can be informative, the utility of these simulations

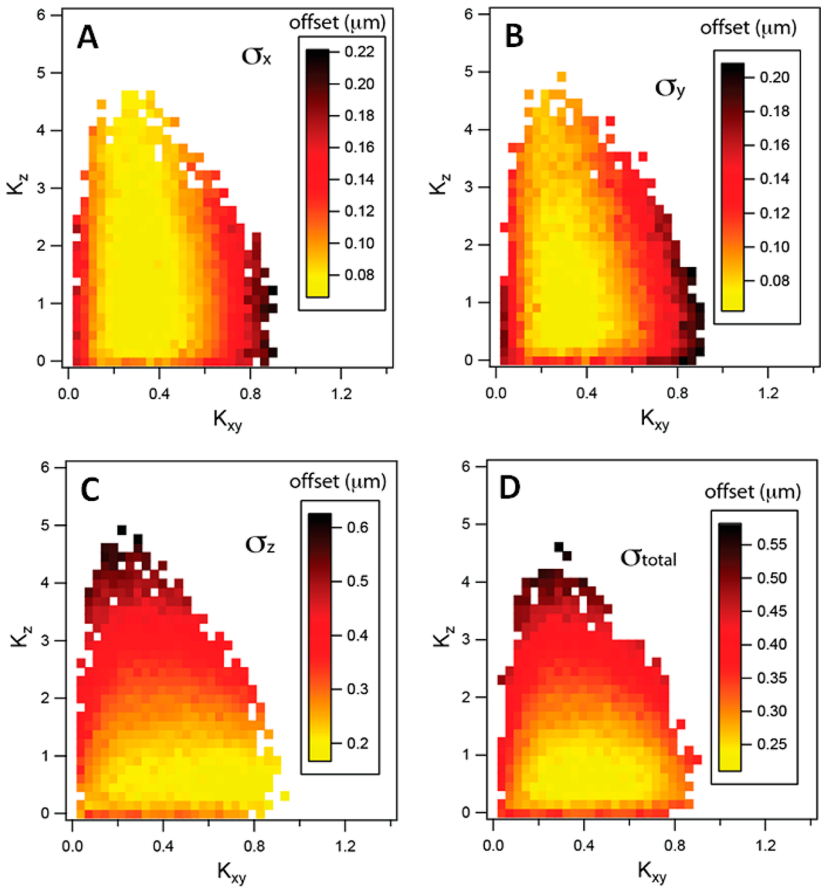

Figure 3. Tracking simulation results over a range of feedback gain parameters (K_{XY}, K_Z) for tracking the Brownian motion of a single fluorescent protein with a diffusion coefficient of 0.5 $\mu m^2/s$. Each pixel in panels A, B, and C represents the root-mean-squared distance (σ) between the molecule position and the stage position for the *X*, *Y*, and *Z* axes, respectively, and a given set of K_{XY}, K_Z values. Panel D is the total root-mean-squared distance of the molecule from the center of the optical probe volume (*i.e.*, $(\sigma_x^2 + \sigma_y^2 + \sigma_z^2)^{1/2}$). A total of twenty 1 s simulation runs were attempted at each value of K_{XY} and K_Z. To be plotted, over half of the simulation runs needed to follow the molecular motion for the duration of the simulation.

lies in testing nearly every feedback parameter to find the optimal system settings for following a molecule of known brightness and/or diffusion coefficient. In order to optimize parameters for tracking GFPs and organic dyes, both of which exhibit significantly lower count rates than QDs, we performed simulations using detection count rates for AG proteins, Rhodamine 110, and Alexa Fluor 488, as well as diffusion coefficients comparable to those experimentally determined by FCS in glycerol/water solutions (*i.e.*, D = 0.5 $\mu m^2/s$). To find optimal feedback parameters, we ran simulations over a wide range of K_X, K_Y, and K_Z values and used the distance between the simulated positions of the molecule and the stage as our performance metric. Values for K_X and K_Y varied between 0 and 1.5 at 0.0375 intervals, while K_Z was varied between 0 and 6 at 0.15 intervals. Twenty simulation runs of 1 s duration were attempted at each K_X, K_Y, K_Z value. Due to the symmetry of our system, for each simulation run, we did not let K_X and K_Y vary independently and always set $K_X = K_Y = K_{XY}$.

Figure 3 shows how the average root-mean-square (rms) distance between the molecule and the stage position varies over the range of tested K_X, K_Y, K_Z values. The rms values for each Cartesian coordinate are plotted in Figure 3A–C, with Figure 3D showing the total rms distance between the molecule and the center of the stage position. As can be seen, our simulations indicate that there is a fairly broad distribution of K_X, K_Y, and K_Z parameters capable of following 3-D motion of individual GFPs diffusing with a diffusion coefficient of 0.5 $\mu m^2/s$. We point out (perhaps not surprisingly) that tracking accuracy in *XY* is relatively unaffected and loosely dependent upon the choice of K_Z, whereas the tracking accuracy in *Z* is similarly insensitive to the value chosen for K_{XY}. We also tested the same range of feedback parameters on molecules exhibiting 3-D Brownian motion at 0.85 and 0.34 $\mu m^2/s$, which spans the range of diffusion coefficients of the Azami Green constructs in 90:10 glycerol/water. These results are shown in Supporting Information Figure S2. Visual inspection and averaging of Figure 3 and Figure S2 was used to obtain optimal *K* values (0.35, 0.35, 0.75) used in our current tracking experiments. We further note that our attempts to include an integral error term in our PID feedback simulations have always returned tracking errors that are worse than simple proportional-based (*i.e.*, no I or D) feedback.

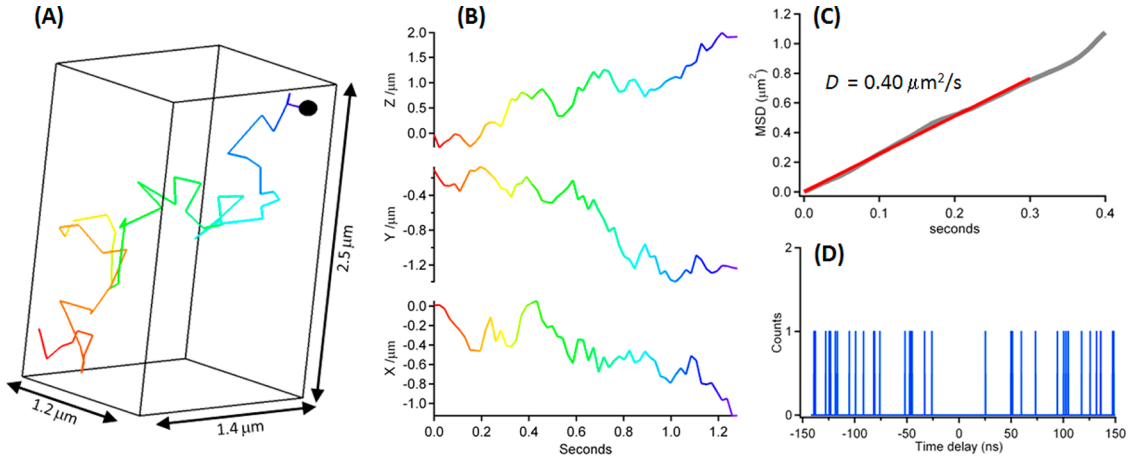

Figure 4. (A) Example of a 3-D trajectory and corresponding (B) *XYZ* piezo stage response, (C) 3-D MSD analysis, and (D) photon pair correlation analysis for a single Rh110 molecule exhibiting Brownian motion in a 96% (wt) aqueous glycerol solution.

Tracking Individual Organic Dyes and Fluorescent Proteins. Regardless of which modality one employs to track a single fluorescent reporter molecule, a general aim is to maximize the per molecule count rate while minimizing undesirable photophysical effects such as photoblinking and photobleaching. For QDs and fluorescent polymeric nanoparticles with an ample photon budget, we can regularly achieve sufficiently high count rates (50−200 kHz) at low laser powers (≤10 μW), enabling tracking of such particles for seconds to minutes.[16,46] However, organic dyes and FPs exhibit markedly poorer photostability than QDs or nanoparticles and thus require careful optimization of the laser power in order to maximize the SNR while minimizing the photobleaching rate. In general, for tracking organic dyes and FPs, we employed excitation powers of 15−30% of the saturation power as determined by fluorescence correlation spectroscopy (FCS).[70] Higher laser powers do yield higher count rates but at the cost of faster photobleaching, which ultimately limits track duration. In addition, we chose to analyze only those tracks with a duration of at least 100 ms (corresponding to twenty 5 ms time steps) and a minimum count rate of 20 kHz. We obtained diffusion coefficients for each track using both mean-squared displacement (MSD)[5] and maximum likelihood estimation (MLE) methods[17] of analysis as described elsewhere.[46]

Figure 4 shows an example of a 3-D trajectory of a single Rhodamine 110 dye molecule diffusing in 96% (wt) aqueous glycerol solutions. Also shown are the corresponding *X*, *Y*, and *Z* piezo stage positions and the 3-D MSD and photon pair correlation histogram for this track. Figure 5 shows histograms of diffusion coefficients determined by MLE analysis, track durations, and photon pair correlations summed across all 721 Rhodamine 110 (Rh110) molecules tracked. Similar histograms for all 557 Alexa Fluor 488 (AF488) molecules tracked are presented in Supporting Information Figure S3. The average diffusion coefficient values for Rh110 and

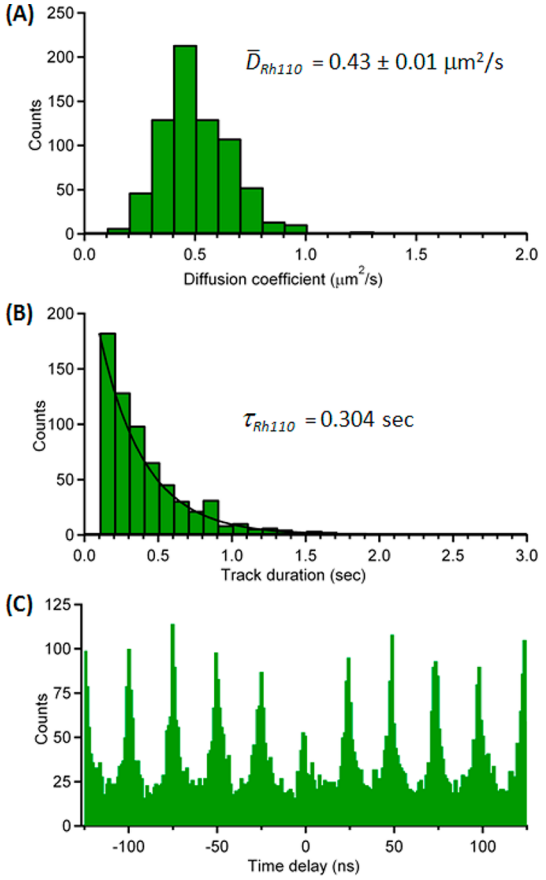

Figure 5. Histograms of (A) diffusion coefficients, (B) track durations, and (C) summed photon pair correlations for all 721 Rh110 molecules tracked in 96% (wt) aqueous glycerol solutions.

AF488 are 0.43 ± 0.01 and 0.49 ± 0.02 $\mu m^2/s$, respectively, with these average values (and their associated error) determined by Gaussian fits to the measured diffusion coefficient distributions. We note the errors on obtaining the central position of the distribution (*i.e.*, ±0.01 $\mu m^2/s$ for Rh110 and ±0.02 $\mu m^2/s$ for AF488) are substantially less than the standard deviation of the

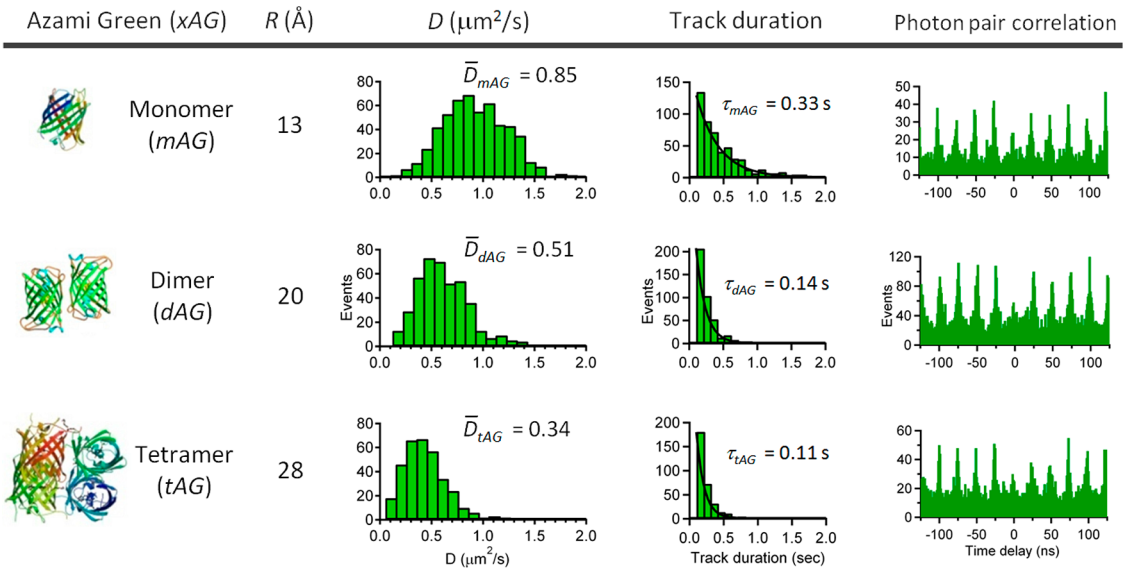

Figure 6. Summary of single-molecule tracking results for Azami Green oligomers mAG, dAG, and tAG in 92% (wt) aqueous glycerol solutions. Data reflect only those tracks ≥100 ms in duration. *R* (Å) is the hydrodynamic radius in angstroms. Diffusion coefficient histograms prepared using the MLE method of analysis. Track duration histograms were fitted with a single exponential. Photon pair correlation histograms represent the sum of all tracks.

distribution of diffusion coefficients, with the standard deviation of the Rh110 diffusion coefficient distribution being 0.17 $\mu m^2/s$ and the standard deviation of the AF488 distribution being 0.25 $\mu m^2/s$. The average values of the diffusion coefficients for Rh110 (0.43 $\mu m^2/s$) and AF488 (0.49 $\mu m^2/s$) determined from MSD analysis are within reasonable agreement of values predicted by the Stokes–Einstein relationship (Supporting Information). Photon antibunching[71,72] is apparent in the summed photon pair correlation histogram (Figure 5C and Supporting Information Figure S3C), indicating that we are tracking single molecules. The small peak at zero time delay is due to the presence of background counts (*e.g.*, Raman scattered laser light) that results in detection of two photons simultaneously.[46,73] This central peak is larger for organic dyes and FPs due to the lower SNR characteristic of organic dyes and FPs compared to QDs. In general, a lower SNR necessitates the use of lower intensity thresholds, thereby allowing a greater percentage of background photons to be counted compared to when we track QDs in pure, low background glycerol/water mixtures. We have previously reported the existence of a similar central peak at zero time delay in the antibunching histogram while tracking single QDs over several micrometers in 3-D in high background environments intentionally designed to degrade the SNR.[46]

For tracking FPs, we chose Azami Green (AG), which is a fluorescent protein from the stony coral, *Galaxeidae*.[74] AG exists as a tetrameric complex (tAG) in nature, with four GFP-like β-barrel subunits. Both its dimeric (dAG) and monomeric (mAG) forms have been directly expressed[70,74] and are stable in solution. In addition, all three AG oligomers show identical absorption and emission spectra similar to GFP (Supporting Information Figure S4), and spectroscopic studies indicate that mAG, dAG, and tAG all behave photophysically as single quantum emitters.[75] Because the hydrodynamic radius increases systematically from mAG (13 Å) to dAG (20 Å) to tAG (28 Å),[75] AG oligomers represent an ideal model system for evaluating the performance of our microscope while tracking FPs.

Figure 6 summarizes tracking results for all AG proteins. Among the 542 mAG tracks, 424 dAG tracks, and 335 tAG tracks analyzed, average diffusion coefficients ranged from 0.35 $\mu m^2/s$ for tAG to 0.85 $\mu m^2/s$ for mAG in 92% (wt) aqueous glycerol solutions, as determined by MSD analysis. The ratio of diffusion coefficients, D_{mAG}/D_{dAG} and D_{mAG}/D_{tAG}, are consistent with ratios of theoretical values, with the measured diffusion coefficients indicating that the mass fraction of glycerol was approximately 90% in all AG oligomer solutions. The relative widths of the diffusion coefficient histograms may be related to the relative errors between the piezo step size and the actual distance traveled by the molecule for the different protein constructs. Larger errors (which would occur for faster diffusing proteins) lead to greater scatter in the MSD plots, which ultimately leads to greater scatter in the slopes of the linear fits. Perhaps surprisingly, the average track duration shows a decreasing trend from mAG to tAG. We initially expected an opposite trend since the likelihood of a molecule escaping the confocal probe volume during a track should be less for larger, slower moving oligomers. However, considering that we utilized a constant laser power (±10%) for all AG oligomers, we speculate that the observed trend is the result of the relative rates of photobleaching and/or photoblinking as determined by the position of the

oligomer within the probe volume during each iteration of a track. That is, since there is rapid energy transfer among the chromophores in the dAG and tAG constructs,[75] the bleaching of any single chromophore in the protein construct effectively quenches the fluorescence of the entire complex, which leads to faster effective bleaching rates for the larger protein constructs. For example, if there is a constant probability, p, that a single AG chromophore will bleach in a given 5 ms period, then the likelihood of acquiring a mAG track "N" 5 ms iterations long is $(1-p)^N$ or $\exp[-N \times \ln(1/(1-p))]$. However, for dAG, if one assumes that each AG chromophore has a similar "p" probability of bleaching during the 5 ms period, the probability that both chromophores are intact after 5 ms is $(1-p)(1-p)$, such that the probability of acquiring a track N iterations long is $(1-p)^{2N}$. Similarly for tAG, the probability of a track N iterations long is $(1-p)^{4N}$. From this simple analysis, one would expect an exponential decay in track durations, with the dAG and tAG decay constants being $2\times$ and $4\times$, respectively, the mAG decay constant. Our measured $1/e$ decay times in track duration (0.33, 0.14, 0.11) for mAG, dAG, and tAG do not follow the 4:2:1 distribution expected from the above simple analysis, but the trend is in right direction, which suggests some agreement with this simple model. We note that in addition to rapid energy transfer among the chromophores potentially leading to larger photobleaching rates for dAG and tAG, there are other reasons these larger oligomers may bleach faster. In particular, because larger, slower moving oligomers can be more tightly tracked, they spend a greater amount of time in or closer to the center of the Gaussian excitation probe volume where excitation intensity is the highest. Coupled with the fact that the laser power at which the first excited state of AG oligomers becomes saturated shows a decreasing trend from mAG to tAG,[70,75] we speculate that, for a given laser power, the rates of photobleaching and photoblinking (*i.e.*, reversible transfer into the dark triplet state) increase from mAG to tAG, resulting in shorter track durations with larger oligomer size.

The decreasing trend in the average diffusion coefficients from mAG to tAG is compelling evidence that we are tracking individual proteins, as we would not expect such a trend if we were tracking randomly sized aggregates. However, a salient feature of our tracking microscope is the ability to record the arrival time of each detected photon and perform post-acquisition time-resolved photon pair correlation analysis in order to determine if the fluorescence signal detected while tracking is arising from a single *versus* multiple quantum emitter.[46] Fluorescence photon antibunching is generally accepted as unequivocal confirmation that a fluorescence signal is arising from a single quantum emitter.[71] As shown in Figure 6, we observed antibunching in the summed photon pair correlation histograms for all three AG oligomers, proving that we are tracking single proteins. As mentioned above for organic dyes, the small peaks observed at zero time delay are due to the low SNR characteristic of FPs, where background counts can begin to obscure the expected antibunching behavior.[73] Our antibunching observations further support that fluorescence emission from dimeric and tetrameric GFP-like oligomers results from nonradiative energy transfer between chromophore centers within each β-barrel.[72,75]

SUMMARY

In this work, we have outlined the details of Monte Carlo simulations used to optimize the feedback parameters of our 3-D tracking microscope and presented data demonstrating that our tracking microscope can follow organic dyes and fluorescent proteins in real-time over several micrometers in solution as they exhibit Brownian motion at rates of up to $\sim 1\ \mu m^2/s$. Although several groups have reported 3-D tracking of QDs and fluorescent nanoparticles over several micrometers in solution, to our knowledge, our work here represents the first demonstration of real-time 3-D tracking of single organic dyes and fluorescent proteins over axial distances routinely greater than $\sim 3\ \mu m$. This specific distance is not simply an arbitrary metric by which to evaluate the technical capabilities of a particular single-molecule tracking system. Rather, it represents an important measure of the potential for a tracking system to visualize and follow small, soluble proteins over the total intracellular space of a living cell. Ultimately, our goal is to be able to track individual proteins across tens of micrometers in 3-D as they traverse through the cytoplasm and across cell membranes in living cells and tissues. Although we performed our experiments in low background glycerol/water solutions, we anticipate that utilizing red-emitting fluorophores, adding reagents to suppress autofluorescence and improve fluorophore photostability, and employing multiphoton excitation to reduce background and phototoxicity will greatly facilitate the extension of our 3-D tracking technology to organic dyes and FPs in living cells and tissues.

We studied Brownian motion of individual organic dyes and individual fluorescent proteins in glycerol/water mixtures such that motion was retarded to rates below $1\ \mu m^2/s$. We note that, although free diffusion within the cytoplasm occurs at much faster rates, several classes of intracellular proteins participate in processes occurring at similar rates of diffusion. As discussed above, such processes include diffusion of mRNA in the nucleus[64] or cytoplasm,[65] transport of proteins through the nuclear pore complex,[34,40] and active motion driven by dynenin or kinesin.[9] We point out that faster tracking speeds are possible by increasing the size of our optical probe volume, but this would lead to a much larger background count rate.

Optimization of the probe volume size (in addition to performing feedback at kilohertz rates) is ongoing as is future areas of research aimed toward our ultimate goal of tracking individual GFPs in 3-D in the cellular cytoplasm or the nucleus.

Lastly, we note that the ability to track single molecules in clean, low background solutions also enables a range of steady-state and time-resolved fluorescence spectroscopic measurements to be performed on single, freely diffusing soluble proteins without the need for immobilization on a substrate. Single-molecule fluorescence spectroscopy performed on labeled biomolecules passing one-by-one through a stationary probe volume is a proven tool to explore heterogeneity in proteins or nucleic acid structures.[76−80] However, in these cases, the molecule is probed only for the few milliseconds that it spends in the probe volume, making long-term measurements on the same molecule impossible. By performing single-molecule spectroscopy on a molecule as it is being tracked, we can extend the observation time by orders of magnitude and observe, for example, conformational changes of freely diffusing proteins by single-molecule Förster resonance energy transfer.[76] Addition of reagents to enhance dye photostability may also further extend observation times and lead to more reliable statistics.[81]

MATERIALS AND METHODS

Materials and Sample Preparation. Rhodamine 110 (Rh110), Alexa Fluor 488, and 525 nm emitting QDs were obtained from Life Technologies. Glycerol was purchased from Sigma Aldrich. All chemicals were used as received without further purification. The mAG, dAG, and tAG were individually expressed in *Escherichia coli* and purified as described previously.[70] No. 1.5 cover glasses were purchased from Corning. Concentrated stock solutions were prepared in either ethanol (Rh110, AF488) or buffer (QDs, name of buffer; AG, PBS) at micromolar concentrations and serially diluted to sub-nanomolar concentrations in glycerol/water mixtures followed by vigorous vortex mixing immediately prior to tracking. Prior to dilution, all stock solutions were centrifuged at 13 000 rpm for 5 min to remove aggregates.

Tracking Microscope. Figure 1 depicts our 3-D confocal, feedback-based single-particle tracking microscope design, which has been described in detail elsewhere.[42] The collimated output of a fiber-coupled 485 nm pulsed diode laser (PicoQuant PD485) operating at 40 MHz is directed into an inverted microscope (IX71, Olympus) by a dichroic beam splitter (Di01-R488-25x36, Semrock) and focused by a water immersion objective (60×, 1.2 NA, Olympus) to a near diffraction-limited spot positioned ∼25 μm above the cover glass surface into the bulk solution. Fluorescence emission is transmitted through the dichroic mirror and filtered through an emission band-pass filter (HQ525, Chroma) before being focused by a 250 mm focal length achromat (Thor Laboratories AC254-250-A) serving as a tube lens.

Fluorescence emission is split 50:50 and imaged onto two identical fiber optic pairs (Polymicro Technologies), each consisting of two 50 μm diameter optical fibers with a center-to-center fiber separation of ∼55 μm. Each fiber acts as a spatial filter (pinhole) for a quad-unit single-photon-counting avalanche photodiode (SPAD) (PerkinElmer SPCM-AQ4C) coupled to each fiber. Axial alignment is achieved by iteratively translating one fiber optic pair while measuring the autocorrelation function of a dilute dye solution with a commercial correlator (ALV 5000E/FAST) until the average counts per fluorophore are maximized. One pair of spatial filters is oriented perpendicular to the other pair and also located at a slightly different distance from the tube lens in order to axially separate the two detection planes, thereby enabling positional sensitivity in *Z*. The distance between the two detection planes is set to ∼250 nm in sample space, determined by raster scans and image analysis on immobilized QD samples. The four spatially arranged fibers form an approximate tetrahedral detection volume in sample space.

Counts from all four SPADs are read by pulse counting electronics (National Instruments PCI-6602, Becker & Hickl SPC630). Active PID feedback is performed for each 5 ms time step in a trajectory by reading the counts on each detector, processing through a LabVIEW Real-Time algorithm, and translating a fast-scanning *XYZ* piezo stage (Physik Instrumente P-733.3DD) to reposition the emitter toward the center of the tetrahedral detection volume. The time-tagged, time-resolved information from the SPC630 is used to post-process photon pair correlation data for each trajectory.

A 3-D collection efficiency function (CEF) was experimentally obtained by acquiring a 3 μm *Z*-image stack scanned through a green-emitting QD (QD525, Life Technologies) immobilized on a cover glass. The *XY* step sizes for each image were 100 nm over a 3 × 3 μm field of view, while the *Z* step size between each image plane was 200 nm.

Data Analysis. Raw photon arrival times were processed with custom-written Fortran 90 code to generate photon pair correlation histograms. One nanosecond binning was used to create the photon pair correlation histograms in all figures. Diffusion coefficients were obtained using mean-squared displacement (MSD) and maximum likelihood estimator (MLE) analyses as described previously.[46] Only tracks exceeding minimum duration (100 ms) and summed intensity (20 kHz) thresholds were processed.

Conflict of Interest: The authors declare no competing financial interests.

Acknowledgment. This work was supported through Los Alamos National Laboratory Directed Research and Development (LDRD) and was performed at the Center for Integrated Nanotechnologies, a U.S. Department of Energy, Office of Basic Energy Sciences user facility at Los Alamos National Laboratory (Contract DE-AC52-06NA25396).

Supporting Information Available: Movies of tracking simulation. Measured piezo step response. Additional simulation results. Histogram results for AF488. Ensemble UV−vis and fluorescence spectra for AG oligomers. Calculation of theoretical diffusion coefficients. This material is available free of charge *via* the Internet at http://pubs.acs.org.

REFERENCES AND NOTES

1. Berg, H. C. How To Track Bacteria. *Rev. Sci. Instrum.* **1971**, *42*, 868–871.
2. Berg, H. C.; Brown, D. A. Chemotaxis in *Escherichia-coli* Analyzed by 3-Dimensional Tracking. *Nature* **1972**, *239*, 500–504.
3. Liu, J.; Gardel, M.; Kroy, K.; Frey, E.; Hoffman, B. D.; Crocker, J. C.; Bausch, A.; Weitz, D. Microrheology Probes Length Scale Dependent Rheology. *Phys. Rev. Lett.* **2006**, *96*, 118104-118101–118104-118104.
4. Barak, L. S.; Webb, W. W. Fluorescent Low-Density Lipoprotein for Observation of Dynamics of Individual Receptor Complexes on Cultured Human-Fibroblasts. *J. Cell Biol.* **1981**, *90*, 595–604.
5. Saxton, M. J.; Jacobson, K. Single-Particle Tracking: Applications to Membrane Dynamics. *Annu. Rev. Biophys. Biomol. Struct.* **1997**, *26*, 373–399.
6. Schmidt, T.; Schutz, G. J.; Baumgartner, W.; Gruber, H. J.; Schindler, H. Imaging of Single Molecule Diffusion. *Proc. Natl. Acad. Sci. U.S.A.* **1996**, *93*, 2926–2929.

7. Kusumi, A.; Sako, Y.; Yamamoto, M. Confined Lateral Diffusion of Membrane Receptors As Studied by Single Particle Tracking (Nanovid Microscopy). Effects of Calcium-Induced Differentiation in Cultured Epithelial Cells. *Biophys. J.* **1993**, *65*, 2021–2040.
8. Gelles, J.; Schnapp, B. J.; Sheetz, M. P. Tracking Kinesin-Driven Movements with Nanometre-Scale Precision. *Nature* **1988**, *331*, 450–453.
9. Kural, C.; Kim, H. D.; Syed, S.; Goshima, G.; Gelfand, V. I.; Selvin, P. R. Kinesin and Dynein Move a Peroxisome *in Vivo*: A Tug-of-War or Coordinated Movement? *Science* **2005**, *308*, 1469–1472.
10. Fujiwara, T.; Ritchie, K.; Murakoshi, H.; Jacobson, K.; Kusumi, A. Phospholipids Undergo Hop Diffusion in Compartmentalized Cell Membrane. *J. Cell Biol.* **2002**, *157*, 1071–1081.
11. Cang, H.; Shan, X. C.; Yang, H. Progress in Single-Molecule Tracking Spectroscopy. *Chem. Phys. Lett.* **2008**, *457*, 285–291.
12. Vrljic, M.; Nishimura, S. Y.; Moerner, W. Single-Molecule Tracking. *Methods Mol. Biol.* **2007**, *398*, 193–219.
13. Saxton, M. J. Single Particle Tracking. In *Fundamental Concepts of Biophysics*; Jue, T., Ed.; Humana Press: New York, 2009; pp 147−169.
14. Yu, J.; Xiao, J.; Ren, X.; Lao, K.; Xie, X. Probing Gene Expression in Live Cells, One Protein Molecule at a Time. *Science* **2006**, *311*, 1600–1603.
15. Dahan, M.; Levi, S.; Luccardini, C.; Rostaing, P.; Riveau, B.; Triller, A. Diffusion Dynamics of Glycine Receptors Revealed by Single-Quantum Dot Tracking. *Science* **2003**, *302*, 442–445.
16. Wells, N. P.; Lessard, G. A.; Goodwin, P. M.; Phipps, M. E.; Cutler, P. J.; Lidke, D. S.; Wilson, B. S.; Werner, J. H. Time-Resolved Three-Dimensional Molecular Tracking in Live Cells. *Nano Lett.* **2010**, *10*, 4732–4737.
17. Montiel, D.; Cang, H.; Yang, H. Quantitative Characterization of Changes in Dynamical Behavior for Single-Particle Tracking Studies. *J. Phys. Chem. B* **2006**, *110*, 19763–19770.
18. Moerner, W.; Fromm, D. P. Methods of Single-Molecule Fluorescence Spectroscopy and Microscopy. *Rev. Sci. Instrum.* **2003**, *74*, 3597–3619.
19. Schütz, G.; Schindler, H.; Schmidt, T. Single-Molecule Microscopy on Model Membranes Reveals Anomalous Diffusion. *Biophys. J.* **1997**, *73*, 1073–1080.
20. Han, J. J.; Boo, D. W. Reversible Immobilization of Diffusive Membrane-Associated Proteins Using a Liquid−Gel Bilayer Phase Transition: A Case Study of Annexin V Monomers. *Langmuir* **2009**, *25*, 3083–3088.
21. Poudel, K. R.; Keller, D. J.; Brozik, J. A. Single Particle Tracking Reveals Corralling of a Transmembrane Protein in a Double-Cushioned Lipid Bilayer Assembly. *Langmuir* **2011**, *27*, 320–327.
22. Sako, Y.; Minoghchi, S.; Yanagida, T. Single-Molecule Imaging of EGFR Signalling on the Surface of Living Cells. *Nat. Cell Biol.* **2000**, *2*, 168–172.
23. Lord, S. J.; Conley, N. R.; Lee, H. D.; Nishimura, S. Y.; Pomerantz, A. K.; Willets, K. A.; Lu, Z.; Wang, H.; Liu, N.; Samuel, R. Dcdhf Fluorophores for Single-Molecule Imaging in Cells. *ChemPhysChem* **2009**, *10*, 55–65.
24. Wells, N. P.; Lessard, G. A.; Phipps, M. E.; Goodwin, P. M.; Lidke, D. S.; Wilson, B. S.; Werner, J. H. Going Beyond 2D: Following Membrane Diffusion and Topography in the IgE−FcεRI System Using 3-Dimensional Tracking Microscopy. *Proc. SPIE* **2009**, 718513.
25. Adler, J.; Shevchuk, A. I.; Novak, P.; Korchev, Y. E.; Parmryd, I. Plasma Membrane Topography and Interpretation of Single-Particle Tracks. *Nat. Methods* **2010**, *7*, 170–171.
26. Bray, D. Signaling Complexes: Biophysical Constraints on Intracellular Communication. *Annu. Rev. Biophys. Biomol. Struct.* **1998**, *27*, 59–75.
27. Miyawaki, A. Visualization of the Spatial and Temporal Dynamics of Intracellular Signaling. *Dev. Cell* **2003**, *4*, 295–305.
28. White, J. A.; Scandalios, J. G. Molecular Biology of Intracellular Protein Trafficking. *Physiol. Plant.* **1988**, *74*, 397–408.
29. Schwartz, A. L. Cell Biology of Intracellular Protein Trafficking. *Annu. Rev. Immunol.* **1990**, *8*, 195–229.
30. Gallagher, K. L.; Benfey, P. N. Not Just Another Hole in the Wall: Understanding Intercellular Protein Trafficking. *Gene. Dev.* **2005**, *19*, 189–195.
31. Lord, S. J.; Lee, H. D.; Moerner, W. Single-Molecule Spectroscopy and Imaging of Biomolecules in Living Cells. *Anal. Chem.* **2010**, *82*, 2192–2203.
32. Kao, H. P.; Verkman, A. Tracking of Single Fluorescent Particles in Three Dimensions: Use of Cylindrical Optics To Encode Particle Position. *Biophys. J.* **1994**, *67*, 1291–1300.
33. Prabhat, P.; Ram, S.; Ward, E. S.; Ober, R. J. Simultaneous Imaging of Different Focal Planes in Fluorescence Microscopy for the Study of Cellular Dynamics in Three Dimensions. *IEEE Trans. Nanobiosci.* **2004**, *3*, 237–242.
34. Yang, W.; Gelles, J.; Musser, S. M. Imaging of Single-Molecule Translocation through Nuclear Pore Complexes. *Proc. Natl. Acad. Sci. U.S.A.* **2004**, *101*, 12887–12892.
35. Prabhat, P.; Ram, S.; Ward, E. S.; Ober, R. J. Simultaneous Imaging of Several Focal Planes in Fluorescence Microscopy for the Study of Cellular Dynamics in 3D. *Proc. SPIE* **2006**, *6090*, 115−121.
36. Holtzer, L.; Meckel, T.; Schmidt, T. Nanometric Three-Dimensional Tracking of Individual Quantum Dots in Cells. *Appl. Phys. Lett.* **2007**, *90*, 1–3.
37. Toprak, E.; Balci, H.; Blehm, B. H.; Selvin, P. R. Three-Dimensional Particle Tracking *via* Bifocal Imaging. *Nano Lett.* **2007**, *7*, 2043–2045.
38. Ram, S.; Prabhat, P.; Chao, J.; Sally Ward, E.; Ober, R. J. High Accuracy 3D Quantum Dot Tracking with Multifocal Plane Microscopy for the Study of Fast Intracellular Dynamics in Live Cells. *Biophys. J.* **2008**, *95*, 6025–6043.
39. Sun, Y.; McKenna, J. D.; Murray, J. M.; Ostap, E. M.; Goldman, Y. E. Parallax: High Accuracy Three-Dimensional Single Molecule Tracking Using Split Images. *Nano Lett.* **2009**, *9*, 2676–2682.
40. Lowe, A. R.; Siegel, J. J.; Kalab, P.; Siu, M.; Weis, K.; Liphardt, J. T. Selectivity Mechanism of the Nuclear Pore Complex Characterized by Single Cargo Tracking. *Nature* **2010**, *467*, 600–603.
41. Berglund, A. J.; Mabuchi, H. Tracking-FCS: Fluorescence Correlation Spectroscopy of Individual Particles. *Opt. Express* **2005**, *13*, 8069–8082.
42. Lessard, G.; Goodwin, P. M.; Werner, J. H. Three Dimensional Tracking of Single Fluorescent Particles. *Proc. SPIE* **2006**, *6092*, 6092051–6092058.
43. Ragan, T.; Huang, H.; So, P.; Gratton, E. 3D Particle Tracking on a Two-Photon Microscope. *J. Fluoresc.* **2006**, *16*, 325–336.
44. Lessard, G. A.; Goodwin, P. M.; Werner, J. H. Three-Dimensional Tracking of Individual Quantum Dots. *Appl. Phys. Lett.* **2007**, *91*, 224106.
45. McHale, K.; Berglund, A. J.; Mabuchi, H. Quantum Dot Photon Statistics Measured by Three-Dimensional Particle Tracking. *Nano Lett.* **2007**, *7*, 3535–3539.
46. Wells, N. P.; Lessard, G. A.; Werner, J. H. Confocal, Three-Dimensional Tracking of Individual Quantum Dots in High-Background Environments. *Anal. Chem.* **2008**, *80*, 9830–9834.
47. Hellriegel, C.; Gratton, E. Real-Time Multi-Parameter Spectroscopy and Localization in Three-Dimensional Single-Particle Tracking. *J. R. Soc. Interface* **2009**, *6*, S3–S14.
48. Juette, M. F.; Bewersdorf, J. Three-Dimensional Tracking of Single Fluorescent Particles with Submillisecond Temporal Resolution. *Nano Lett.* **2010**, *10*, 4657–4663.
49. Pavani, S. R. P.; Thompson, M. A.; Biteen, J. S.; Lord, S. J.; Liu, N.; Twieg, R. J.; Piestun, R.; Moerner, W. Three-Dimensional, Single-Molecule Fluorescence Imaging Beyond the Diffraction Limit by Using a Double-Helix Point Spread Function. *Proc. Natl. Acad. Sci. U.S.A.* **2009**, *106*, 2995–2999.
50. Lew, M. D.; Lee, S. F.; Badieirostami, M.; Moerner, W. Corkscrew Point Spread Function for Far-Field Three-Dimensional Nanoscale Localization of Pointlike Objects. *Opt. Lett.* **2011**, *36*, 202–204.
51. Schütz, G. J.; Pastushenko, V. P.; Gruber, H. J.; Knaus, H. G.; Pragl, B.; Schindler, H. 3D Imaging of Individual Ion

Channels in Live Cells at 40 nm Resolution. *Single Mol.* **2000**, *1*, 25–31.
52. Chen, Y.; Vela, J.; Htoon, H.; Casson, J. L.; Werder, D. J.; Bussian, D. A.; Klimov, V. I.; Hollingsworth, J. A. ″Giant″ Multishell CdSe Nanocrystal Quantum Dots with Suppressed Blinking. *J. Am. Chem. Soc.* **2008**, *130*, 5026–5027.
53. Vela, J.; Htoon, H.; Chen, Y.; Park, Y.; Ghosh, Y.; Goodwin, P.; Werner, J.; Wells, N.; Casson, J.; Hollingsworth, J. Effect of Shell Thickness and Composition on Blinking Suppression and the Blinking Mechanism in ″Giant″ CdSe/CdS Nanocrystal Quantum Dots. *J. Biophotonics* **2010**, *3*, 706–717.
54. Derfus, A. M.; Chan, W. C. W.; Bhatia, S. N. Intracellular Delivery of Quantum Dots for Live Cell Labeling and Organelle Tracking. *Adv. Mater.* **2004**, *16*, 961–966.
55. Medintz, I. L.; Uyeda, H. T.; Goldman, E. R.; Mattoussi, H. Quantum Dot Bioconjugates for Imaging, Labelling and Sensing. *Nat. Mater.* **2005**, *4*, 435–446.
56. Smith, A. M.; Duan, H.; Mohs, A. M.; Nie, S. Bioconjugated Quantum Dots for *In Vivo* Molecular and Cellular Imaging. *Adv. Drug Delivery Rev.* **2008**, *60*, 1226–1240.
57. Shimomura, O. The Discovery of Aequorin and Green Fluorescent Protein. *J. Microsc.* **2005**, *217*, 3–15.
58. Griffin, B. A.; Adams, S. R.; Tsien, R. Y. Specific Covalent Labeling of Recombinant Protein Molecules inside Live Cells. *Science* **1998**, *281*, 269–272.
59. Johnsson, N.; Johnsson, K. Chemical Tools for Biomolecular Imaging. *ACS Chem. Biol.* **2007**, *2*, 31–38.
60. Cabantous, S.; Terwilliger, T. C.; Waldo, G. S. Protein Tagging and Detection with Engineered Self-Assembling Fragments of Green Fluorescent Protein. *Nat. Biotechnol.* **2005**, *23*, 102–107.
61. Patterson, G. H.; Lippincott-Schwartz, J. A Photoactivatable GFP for Selective Photolabeling of Proteins and Cells. *Science* **2002**, *297*, 1873–1877.
62. Ando, R.; Hama, H.; Yamamoto-Hino, M.; Mizuno, H.; Miyawaki, A. An Optical Marker Based on the UV-Induced Green-to-Red Photoconversion of a Fluorescent Protein. *Proc. Natl. Acad. Sci. U.S.A.* **2002**, *99*, 12651–12656.
63. Swaminathan, R.; Hoang, C. P.; Verkman, A. Photobleaching Recovery and Anisotropy Decay of Green Fluorescent Protein GFP-S65T in Solution and Cells: Cytoplasmic Viscosity Probed by Green Fluorescent Protein Translational and Rotational Diffusion. *Biophys. J.* **1997**, *72*, 1900–1907.
64. Shav-Tal, Y.; Darzacq, X.; Shenoy, S. M.; Fusco, D.; Janicki, S. M.; Spector, D. L.; Singer, R. H. Dynamics of Single mRNPs in Nuclei of Living Cells. *Science* **2004**, *304*, 1797–1800.
65. Fusco, D.; Accornero, N.; Lavoie, B.; Shenoy, S. M.; Blanchard, J. M.; Singer, R. H.; Bertrand, E. Single mRNA Molecules Demonstrate Probabilistic Movement in Living Mammalian Cells. *Curr. Biol.* **2003**, *13*, 161–167.
66. Pollard, T. D.; Mooseker, M. S. Direct Measurement of Actin Polymerization Rate Constants by Electron Microscopy of Actin Filaments Nucleated by Isolated Microvillus Cores. *J. Cell Biol.* **1981**, *88*, 654–659.
67. Dix, J. A.; Verkman, A. Crowding Effects on Diffusion in Solutions and Cells. *Annu. Rev. Biophys.* **2008**, *37*, 247–263.
68. Enderlein, J. Theoretical Study of Detection of a Dipole Emitter through an Objective with High Numerical Aperture. *Opt. Lett.* **2000**, *25*, 634–636.
69. Qian, H.; Elson, E. L. Analysis of Confocal Laser-Microscope Optics for 3-D Fluorescence Correlation Spectroscopy. *Appl. Opt.* **1991**, *30*, 1185–1195.
70. Dai, M.; Fisher, H. E.; Temirov, J.; Kiss, C.; Phipps, M. E.; Pavlik, P.; Werner, J. H.; Bradbury, A. R. M. The Creation of a Novel Fluorescent Protein by Guided Consensus Engineering. *Protein Eng., Des. Sel.* **2007**, *20*, 69–79.
71. Kimble, H.; Dagenais, M.; Mandel, L. Photon Antibunching in Resonance Fluorescence. *Phys. Rev. Lett.* **1977**, *39*, 691–695.
72. Sánchez-Mosteiro, G.; Koopman, M.; van Dijk, E. M. H. P.; Hernando, J.; van Hulst, N. F.; García-Parajó, M. F. Photon Antibunching Proves Emission from a Single Subunit in the Autofluorescent Protein Dsred. *ChemPhysChem* **2004**, *5*, 1782–1785.
73. Weston, K. D.; Dyck, M.; Tinnefeld, P.; Muller, C.; Herten, D. P.; Sauer, M. Measuring the Number of Independent Emitters in Single-Molecule Fluorescence Images and Trajectories Using Coincident Photons. *Anal. Chem.* **2002**, *74*, 5342–5349.
74. Karasawa, S.; Araki, T.; Yamamoto-Hino, M.; Miyawaki, A. A Green-Emitting Fluorescent Protein from Galaxeidae Coral and Its Monomeric Version for Use in Fluorescent Labeling. *J. Biol. Chem.* **2003**, *278*, 34167–34171.
75. Temirov, J.; Werner, J. H.; Goodwin, P. M.; Bradbury, A. R. M. ″Sizing″ the Oligomers of Azami Green Fluorescent Protein with FCS and Antibunching. *Proc. SPIE* **2012**, *8228*, 822801–822810.
76. Deniz, A. A.; Dahan, M.; Grunwell, J. R.; Ha, T.; Faulhaber, A. E.; Chemla, D. S.; Weiss, S.; Schultz, P. G. Single-Pair Fluorescence Resonance Energy Transfer on Freely Diffusing Molecules: Observation of Forster Distance Dependence and Subpopulations. *Proc. Natl. Acad. Sci. U.S.A.* **1999**, *96*, 3670.
77. Schuler, B.; Lipman, E. A.; Eaton, W. A. Probing the Free-Energy Surface for Protein Folding with Single-Molecule Fluorescence Spectroscopy. *Nature* **2002**, *419*, 743–747.
78. McCarney, E. R.; Werner, J. H.; Bernstein, S. L.; Ruczinski, I.; Makarov, D. E.; Goodwin, P. M.; Plaxco, K. W. Site-Specific Dimensions across a Highly Denatured Protein: A Single Molecule Study. *J. Mol. Biol.* **2005**, *352*, 672–682.
79. Werner, J. H.; Joggerst, R.; Dyer, R. B.; Goodwin, P. M. A Two-Dimensional View of the Folding Energy Landscape of Cytochrome c. *Proc. Natl. Acad. Sci. U.S.A.* **2006**, *103*, 11130–11135.
80. Werner, J. H.; McCarney, E. R.; Keller, R. A.; Plaxco, K. W.; Goodwin, P. M. Increasing the Resolution of Single Pair Fluorescence Resonance Energy Transfer Measurements in Solution *via* Molecular Cytometry. *Anal. Chem.* **2007**, *79*, 3509–3513.
81. Rasnik, I.; McKinney, S. A.; Ha, T. Nonblinking and Long-Lasting Single-Molecule Fluorescence Imaging. *Nat. Methods* **2006**, *3*, 891–893.